Terraced spreading mechanisms for chain molecules

Umberto D'Ortona and Joël De Coninck
Université de Mons-Hainaut, Faculté des Sciences, 20 place du Parc, 7000-Mons, Belgium

Joel Koplik
Benjamin Levich Institute and Department of Physics, City College of the City University of New York, New York, New York 10031

Jayanth R. Banavar
Department of Physics and Center for Materials Physics, The Pennsylvania State University, University Park, Pennsylvania 16802
(Received 12 December 1994)

The behavior of monomolecular layers of fluid spreading on a solid substrate is examined using molecular dynamics simulations of polymerlike liquids. We consider drops of chain molecules of lengths 8 and 16, composed of Lennard-Jones atoms bound by confining potentials, spreading on an atomic solid substrate. Different strengths of the solid-fluid interaction are studied, in cases where a spreading drop forms distinct layers. We emphasize the conformational properties of the molecules while spreading and the dynamics of the individual layers. In particular, the questions of interlayer mass transfer and permeability are examined in the light of theoretical models.

PACS number(s): 61.20.Ja, 68.10.Gw, 68.45.Gd

I. INTRODUCTION

A number of recent experiments [1–3], computer simulations [4–12], and theoretical models [13,14] have addressed the unusual phenomenon of "terraced" spreading, in which certain polymeric liquids spread completely on certain solid substrates in the form of well-defined monomolecular layers. The experiments have provided the time-dependent profiles of macroscopic drop shapes, but no information on the internal dynamics.

The computer simulations have shown how the solid-fluid interactions can produce a terraced spreading regime, for relatively simple molecules at least, and have indicated a variation of spreading rate with molecule size for large systems. The theoretical work of de Gennes and Cazabat [13] has modeled the layers as rubberlike sheets evolving under disjoining pressure and friction, whose growth originates from mass transfer occurring at their edges. To date, these models have been tested only in an indirect fashion, by verifying the consistency of model parameters with observation.

In this paper, we discuss the results of further molecular dynamics (MD) simulations of the spreading of chain molecules, with two aims. First, we consider how the conformational statistics of the chains are modified by the presence of the substrate and by the spreading process. We have considered chains composed of Lennard-Jones atoms strung together by pairwise confining interactions, whose spreading dynamics on atomic solid substrates has been shown [10] to be consistent with observation in terms of layered structure and growth rate. Such simulations provide detailed information at the atomic level concerning the individual atoms and molecules, and here we use this data base to examine the changes in molecular structure during spreading. We have considered chains of lengths 8 and 16 and several strengths of the solid-fluid interaction potential. Second, we use the simulations to attempt to bridge the gap between theory and experiment, by examining the internal dynamics and molecular motion within and between the layers. In particular, we attempt to quantify the mass transfer between spreading layers in some detail, as this is a key ingredient in modeling.

Section II reviews the MD simulation method, emphasizing the binding that gives rise to polymerlike chains. Section III discusses the statistics of chain conformation in spreading and Sec. IV analyzes the dynamics of the layers. Conclusions and an outlook appear in Sec. V.

II. SIMULATION METHOD

The molecular dynamics algorithm and interactions used in this study are basically of the Lennard-Jones form used in the earlier simulations reported in [7,8], but with the major difference that the fluid is made of *chains* of atoms of lengths 8 and 16. The use of chains is intended to bring the computer models studied closer to the experiments, which involved polymeric fluids such as polydimethylsiloxane (PDMS). A realistic polymer of course contains more than 16 monomers, but it appears that with this number of monomers we can consider enough of these molecules to obtain satisfactory statistics in a reasonable amount of computation time. The basic interaction between all pairs of atoms is of the 6-12 Lennard-Jones type

$$V_{ij}(r)=4\epsilon\left[c_{ij}\left[\frac{r}{\sigma}\right]^{-12}-d_{ij}\left[\frac{r}{\sigma}\right]^{-6}\right], \tag{1}$$

with adjustable coefficients c,d chosen to ensure coexisting heterogeneous phases of solid and liquid. In (1), ϵ and

σ are energy and length scales, respectively, and i,j represent the solid and liquid species. The fluid atoms are readily grouped into chains with the additional pairwise confining potential

$$V_{\text{mol}}(r)=f_{\text{mol}}\left[\frac{r}{\sigma}\right]^{+6} \tag{2}$$

between adjoining atoms. Aside from generating larger molecules than the monoatomic or diatomic systems considered previously [7–9], the chain structure has the effect of strongly reducing the volatility of the fluid so as to bring the simulation closer to the "dry spreading" seen in the experiments, which was not always the case previously. The substrate is a lattice made of one layer of fcc unit cells, whose atoms execute thermal oscillations about their lattice sites, but which retains a solid structure by means of a deep and narrow potential well. (The mass of the solid atoms is chosen to be as many as 50 times that of the fluid so as to have comparable time scales for the atomic motion in fluid and solid, permitting a longer time step in the integration of the equations of motion.)

For computational convenience, the tail of the potentials are cut off at $r_c=2.5\sigma$. The loss of the tail of the fluid-fluid interaction simply changes the transport coefficients of the fluid [15], but since van der Waals forces are known to be significant in spreading we take the precaution of restoring the long-range tail by adding a "wall-averaged" long-range van der Waals–like potential

$$V_{\text{tail}}(r)=A\epsilon\left[\frac{\sigma}{r+u}\right]^{\delta}, \tag{3}$$

where u is the solid lattice constant. Notice that an interaction of this form arises from integrating over a half-space of Lennard-Jones potentials. The coefficients were chosen as $A=1.13$ and $\delta=3$, and we have also considered the cases where $A=20$ and $\delta=4$, as well as no long-range interaction at all. We find that our results are rather insensitive to the amplitude and the power of the long-range potential. In a macroscopic calculation, the van der Waals potential is crucial, but in the very small systems studied here, the short-range part provides the dominant effect.

The basic interaction parameters are chosen as $c_{ff}=d_{ff}=1$ (the standard Lennard-Jones values), $c_{ss}=36.45$, and $d_{ss}=5$ (for an incommensurate solid lattice) and we have considered cases where $c_{sf}=d_{sf}=1$, 2, and 5. This choice of simple potentials does not have the pretension to represent a real PDMS polymer, but nevertheless it contains the basic ingredients to reproduce satisfactorily the experimental results. Given the potential, the motion follows from integrating Newton's equations, using a fifth-order predictor-corrector algorithm. In the remainder of the paper, we nondimensionalize by using σ, ϵ, and the fluid monomer mass as the units of distance, energy, and mass, respectively. The resulting natural time unit is $\tau=\sigma(m/\epsilon)^{1/2}$.

We have considered fluid drops made initially of 16 384 and 32 000 atoms in chains of length 8 or 16. Initially, the fluid atoms are placed on fcc lattice sites at density 0.8 and the resulting drop is allowed to equilibrate until its properties stabilize. Constant kinetic-energy rescaling is used to maintain a temperature $T=1$ during this stage. Independently, substrates made of a single layer of fcc cells at density 2.7 of up to 147 456 atoms are equilibrated at the same T. After equilibration, the drop is given a small downward velocity and the substrate interaction is turned on. Once within interaction range of the solid, the drop is drawn down to the surface by the interatomic forces and begins to spread. During spreading, the temperature is kept constant by continued equilibration of the solid alone, which is, from our point of view, the procedure closest to the experiment. Thus the temperature of the solid is exactly constant and the temperature of the liquid varies by less than 10% over the entire experiment.

III. CONFORMATIONAL PROPERTIES OF THE CHAINS

A typical drop undergoing terraced spreading is shown in Fig. 1 from side and top views. In this case the drop is

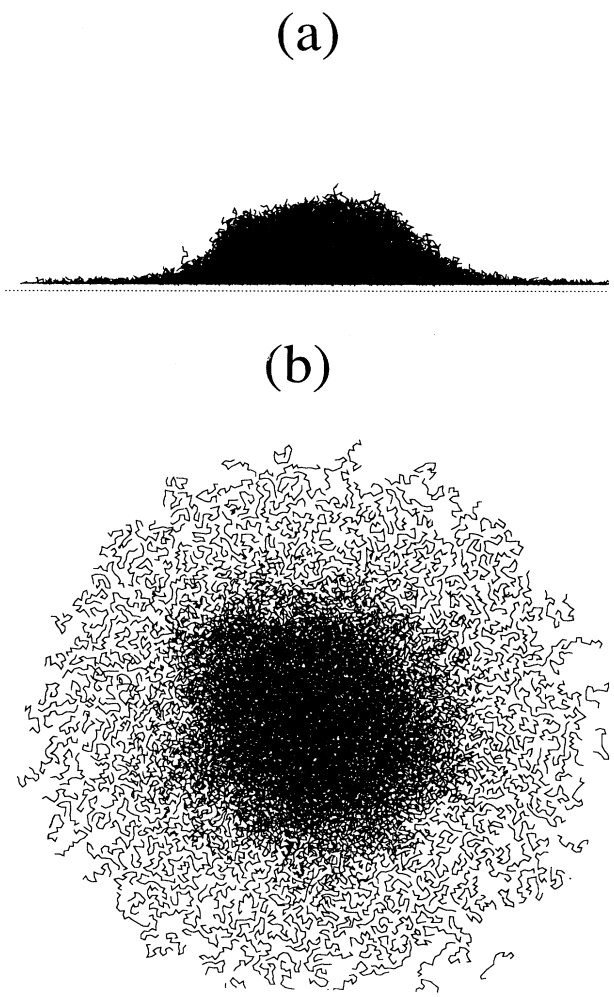

FIG. 1. (a) Side view of a drop of 2000 16-atom molecules during spreading. (b) The associated top view.

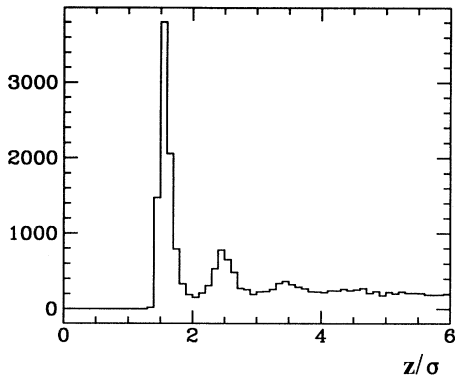

FIG. 2. Number of atoms as a function of their height z for the snapshot given in Fig. 1.

made of 2000 16-atom chains, with solid-fluid attraction coefficients $c_{sf}=d_{sf}=1$. One may note the absence of vapor and the distinct layering near the wall. The layering may be quantified by constructing a histogram of the number of molecules as a function of vertical position z. Figure 2 gives the histogram corresponding to the previous snapshot, which clearly shows the existence of several layers, each of thickness approximately 0.8 (in units of σ). More precisely, the top of the solid is at $z=1.14$, a very pronounced first fluid layer extends from $z=1.4$ to 2.2, a second extends from that height to $z=3.0$, and a third up to 3.9. At later times, the layering persists while the relative heights of the different peaks change due to the spreading of the drop. Other cases of spreading drops show a very similar distribution of peaks, and in the remainder of this article we will define the first layer as those fluid particles with $z \leq 2.2$.

Next we consider the coverage of the substrate by the first layer. Overall, the fluid density is roughly constant but trails smoothly off near the edges. We illustrate this behavior in Fig. 3, which gives the radial distribution corresponding to the snapshot discussed above. As the drop

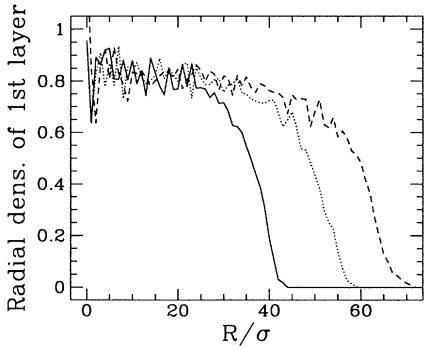

FIG. 3. Radial density (i.e., per unit of surface) for the first layer of the drop shown in Fig. 1.

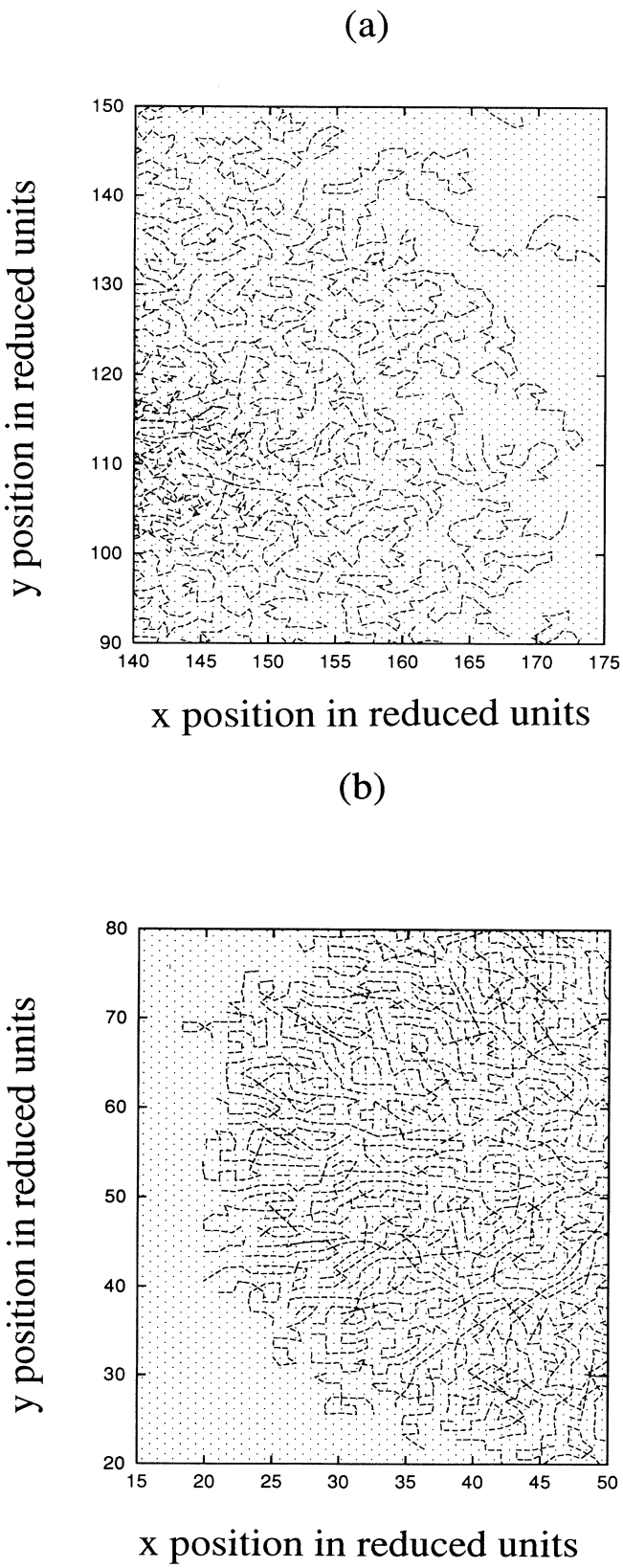

FIG. 4. Blowup of a portion of the first layer of a spreading drop: (a) $c_{fs}=d_{fs}=1$ and (b) $c_{fs}=d_{fs}=5$.

spreads, the central plateau moves outward in radius, with no significant change in height, confirming that the first layer remains compact during the spreading. Again, for drops with other parameters, the same behavior is observed. Locally, the structure of the first layer shows the atoms in a molecule attempting to fall into the potential minima associated with the substrate and so on for the other layers. In Fig. 4(a) we show a zoom view of a part of Fig. 1(b), with the fluid molecule positions superposed on the substrate atom sites. The arrangement of fluid molecules with respect to the wall changes with the solid-fluid interaction strength; in Fig. 4(b), we give the corresponding figure for the case $c_{sf}=d_{sf}=5$. Here the fluid structure is more solidlike and resembles a square lattice.

A further aspect of the wall coverage is the degree to which a fluid molecule is *entirely* within the first layer. In Fig. 5(a) we show as a function of time, separately for chains of length 8 and 16, the fraction of molecules in the drop that have at least one atom in the first layer and in Fig. 5(b) the fraction of molecules with all atoms in the first layer. We see that with shorter chains the covering is much more effective and at the same time the covering with the polymer is much more rapid.

To assess the distortion of the molecule shape resulting

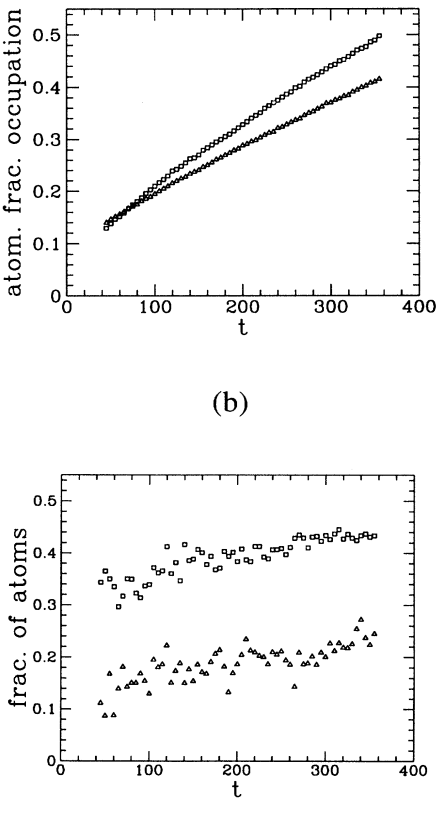

FIG. 5. (a) Atomic fractional occupation of the first layer as a function of the time for 1024 16-atom chains (△) and for 2048 8-atom chains (□) and (b) the fraction of atoms for which the associated molecules entirely belong to the first layer as a function of the time.

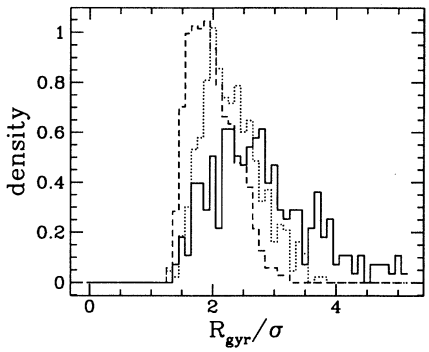

FIG. 6. Density of radius of gyration for the free drop (dashed line), for the first layer corresponding to $c_{fs}=d_{fs}=1$ (dotted line), and for the first layer corresponding to $c_{fs}=d_{fs}=5$ (solid line).

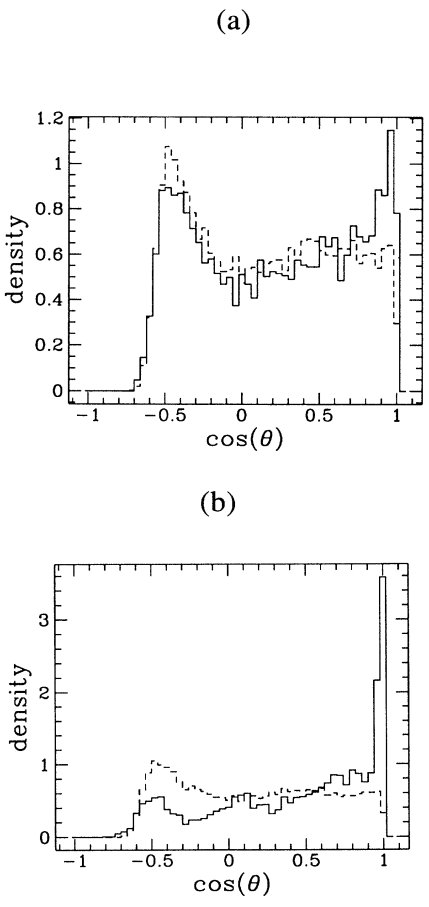

FIG. 7. Density of bond angles for (a) $c_{sf}=d_{sf}=1$ and (b) $c_{sf}=d_{sf}=5$.

from spreading along the wall, we have measured the radius of gyration R_{gyr} and the bond angles θ of the chains. In Fig. 6 we give the histograms of the radius of gyration of the molecules for the free drop after equilibration and for the first layer at the end of the simulation (time 515τ) for the case of length-16 chains with $c_{sf}=d_{sf}=1$ and 5. We see that the molecules of the first layer tend to elongate, as one would anticipate from the fact that the fluid atoms attempt to find uncovered wall sites. The average radius of gyration increases from 2.018 in the free drop to 2.541 in the first spreading layer. As the wall-fluid attraction increases, the histograms indicate an increase in the average radius of gyration.

The molecular orientations can be further quantified through a histogram of the cosine of the angle θ between adjacent bonds along a chain; see Fig. 7(a) for $c_{sf}=d_{sf}=1$ and Fig. 7(b) for $c_{sf}=d_{sf}=5$. In the free drop, there is a tendency for the angle to be 120°, corresponding to three atoms at their respective potential minima. In the first layer of the spreading drop, on the other hand, the favored angle is 0°, consistent with the aforementioned behavior of the radius of gyration.

Finally, as a simple measure of the degree to which the molecules are pinned by the wall potential, we have computed the mean-square displacement $D^2(t)$ of atoms in the first layer as a function of time over 20 000 time steps for the atoms that remain in the first layer during that period. We have measured $D^2(c_{sf}=d_{sf}=1)=40.83$ in reduced units $D^2(c_{sf}=d_{sf}=2)=12.22$ and $D^2(c_{sf}=d_{sf}=5)=1.37$, while the mean-square displacement for the atoms far from the wall is of order 40. We thus see that increasing the wall potential reduces the atomic displacements and, furthermore, for the case $c_{sf}=d_{sf}=5$, the fluid appears to be quite pinned in place.

IV. DYNAMICS OF THE LAYERS

We now turn to a consideration of the spreading layers, treated as continua. In Fig. 8 we plot $N_i(t)$, the number of atoms in the ith layer ($i=1,\ldots,4$) as a function of time after equilibration, for the largest drop made by 2000 16-atom chains. Note that, in view of the constant density within a layer, the number of atoms in a layer is proportional to the layer radius squared. The linear behavior for the first layer is entirely compatible with the diffusive growth law $N_1 \sim R_1^2 \sim t$, seen in experiment [1] and in Monte Carlo models [6]. For the other layers, the spreading behavior is less clear, presumably due to finite-size effects. Thermodynamically, the ultimate equilibrium state is a single layer atop the substrate and the upper layers should eventually disappear. Indeed, in the corresponding plot for layer growth in the smaller system of 2048 8-atom chains in Fig. 9, one sees the second, third, etc., layers grow transiently before they are depleted in favor of the first layer.

The most developed theoretical model for terraced spreading, due to de Gennes and Cazabat [13], approximates the layers as rubberlike sheets driven by van der Waals forces from the substrate, restrained by interlayer friction, and with mass transfer between them occurring near the edges in the "permeation ring." To examine the basis of this model, as well as to provide some general insight into the dynamics of the layers, we have studied the interlayer transport in some detail.

First, following previous studies [7,8], we have computed the probability distributions for vertical and horizontal displacements in the *second* layer, for 16-atom chains at $c_{fw}=d_{fw}=1$. The layer is divided into four annular rings $0\le R\le 10$, $10\le R\le 20$, $20\le R\le 30$, and $30\le R\le 40$, where R is the distance between the atom and the center of the layer (roughly the axis of symmetry of the drop). For each ring, we compute the histogram of radial (Fig. 10) and vertical (Fig. 11) displacements, over a time interval of 100τ.

As in previous work, we see that the radial growth and vertical motion are greatest at the edges (see curve 3 in Figs. 10 and 11), but that some motion occurs in all parts of the layer. Since more holes in the first layer and vacant wall sites are available at the edges, the behavior in

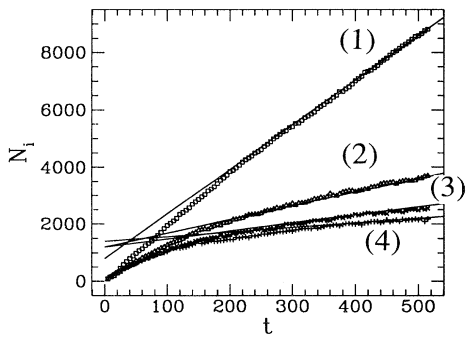

FIG. 8. $N_1(t)$, $N_2(t)$, $N_3(t)$, and $N_4(t)$, the number of atoms in the first, second, third, and fourth layers, respectively, as a function of time in units of τ after equilibration, for the largest drop made of 2000 16-atom chains. The different straight lines correspond, respectively, to $15.6t+800$, $4.8t+1200$, $2.8t+1200$, and $1.6t+1400$.

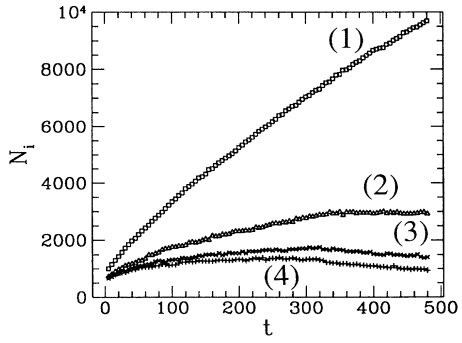

FIG. 9. $N_1(t)$, $N_2(t)$, $N_3(t)$, and $N_4(t)$, the number of atoms in the first, second, third, and fourth layers, respectively, as a function of time in units of τ after equilibration, for the drop made by 2048 8-atom chains.

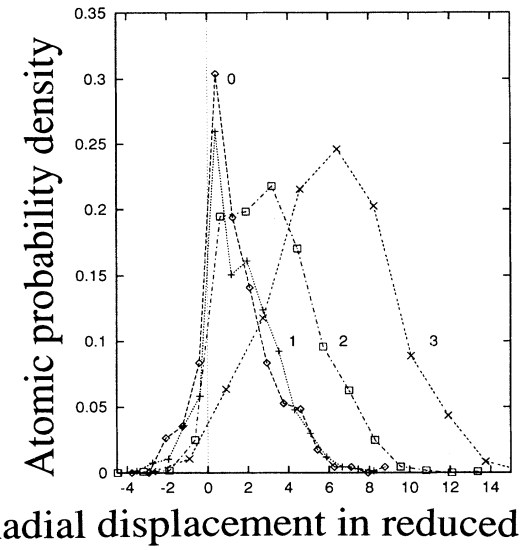

FIG. 10. Atomic probability density for radial displacement $\Delta r = r\ (t=515\tau) - r\ (t=415\tau)$ for the four regions $30 \le r\ (t=415\tau) \le 40$, $20 \le r\ (t=415\tau) \le 30$, $10 \le r\ (t=415\tau) \le 20$, and $0 \le r\ (t=415\tau) \le 10$ (indicated, respectively, by 3, 2, 1, and 0 on the figure) associated with the atoms that belong to the second layer at time $t=415\tau$.

Fig. 11 is entirely reasonable. Note also that some radial drift occurs for even the atoms belonging to the inner rings.

An alternative measure of mass transfer is obtained by plotting the histogram of the radii where atoms of the second layer enter the first layer, normalized by the ra-

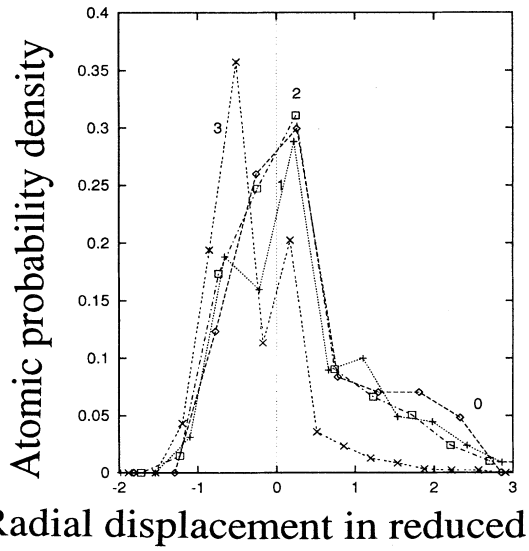

FIG. 11. Atomic probability density for vertical displacement $\Delta z = z\ (t=515\tau) - z\ (t=415\tau)$ for the four regions $30 \le r\ (t=415\tau) \le 40$, $20 \le r\ (t=415\tau) \le 30$, $10 \le r\ (t=415\tau) \le 20$, and $0 \le r\ (t=415\tau) \le 10$ (indicated, respectively, by 3, 2, 1, and 0 on the figure) associated with the atoms that belong to the second layer at time $t=415\tau$.

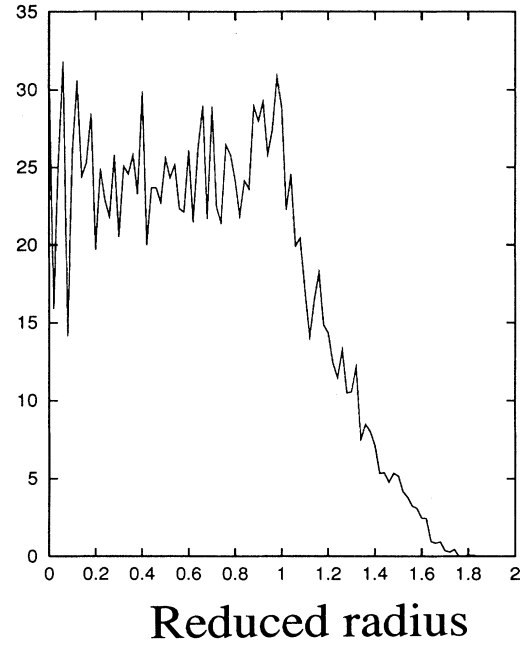

FIG. 12. Histogram of the radius R of the entry point of the atoms of the second layer going into the first layer divided by the radius of the second layer at that time $R_2(t)$ between $t=415\tau$ and 515τ.

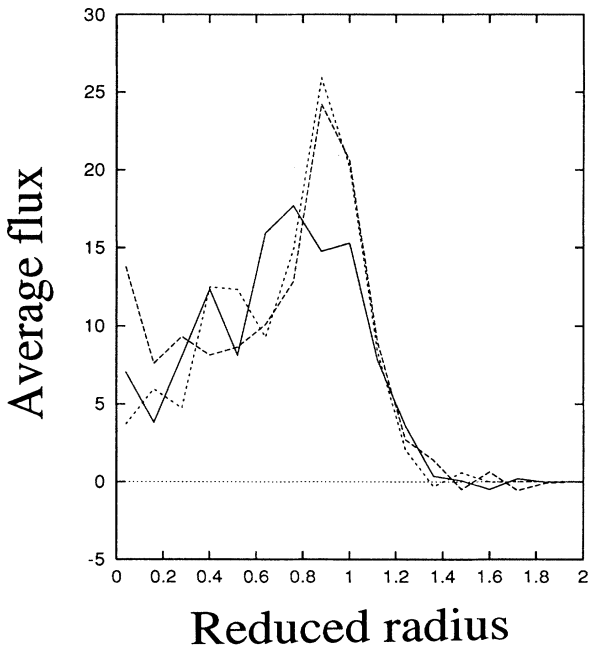

FIG. 13. Average flux over 100τ per unit of area of atoms of the 2000 16-atom drop going from the second layer into the first layer as a function of the radius R divided by the radius of the second layer at that time $R_2(t)$ for three different starting times $t=145\tau$ (solid line), $t=245\tau$ (dashed line), and $t=345\tau$ (dotted line).

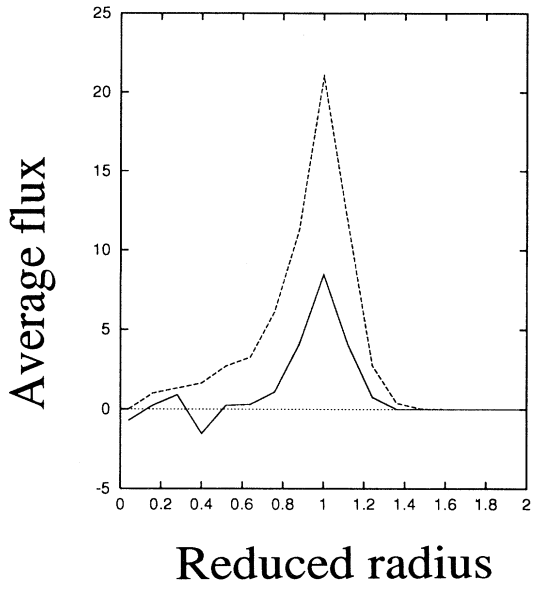

FIG. 14. Average flux over 100τ between the first and second layer for a drop of 1024 16-atom chains with $c_{sf}=d_{sf}=5$ versus the reduced radius R^* for two different starting times $t=610\tau$ (solid line) and $t=510\tau$ (dotted line).

dius of the second layer at that time, taken over the final 100τ of the simulations; see Fig. 12. (If instead we plot the histograms of the displacements of the molecular center of mass, a very similar result is found.) In this case we see a very broad distribution that cuts off only near the layer's edge. This result may seem to be in contradiction to the previous plots. To clarify the situation, we have studied the characteristics of the *flux* of atoms passing through a plane at $z=2.2$ separating the first and the second layers. Atoms moving downward from the second to the first layer are weighted by $+1$ while atoms moving upwards are weighted by -1. To improve the statistics, we average over three 100τ time intervals beginning at initial times 215τ, 315τ, and 415τ and in each case plot the result as a function of the relative radius $R^*=R/R_2$, where R_2 is the mean radius of the second layer at the time of transition. The flux is plotted in Fig. 13 and we see that the flux is much reduced in the central region.

A plausible physical picture of these results is that there are *atomic* fluctuations from layer to layer somewhat broadly distributed in radius, but it is difficult for an entire *molecule* to make a transition in the interior where room is tight. In consequence, the atoms diffuse both up and down, with comparable likelihood. However, at the edge of the layer, where more vacancies are available below, vertical molecular movement is easier. When stronger solid-fluid interactions are used, the tendency for mass transfer to occur near the edge is reinforced (see Fig. 14).

Although movement near the edge of the layer is thus preferred, the validation of the de Gennes–Cazabt model is somewhat ambiguous. While the distribution in Fig. 13 peaks at $R^*\approx 1$, the peak is rather broad. The model leads to the concept of a permeation ring whose width depends on a number of ill-known parameters, where the mass transfer should occur exclusively. Here the permeable region includes most of the area of the layer. The simulation results are thus in qualitative agreement with the de Gennes–Cazabat picture of a permeation ring. It is possible that the study of longer chains or larger drops would improve the agreement, but our computational resources do not permit this.

V. CONCLUSION

We have conducted MD simulations of the spreading of polymerlike fluid chains on atomically smooth solid substrates. The results of the simulations are consistent with experiment, in terms of the presence of well-defined molecular monolayers during spreading and the rate with which the layers grow in time. The detailed microscopic information provided here has allowed us to study the internal dynamics of the molecules and the layers they comprise and to examine the basis of theoretical models for the process.

Earlier calculations on simpler molecular systems [7,8] also exhibited terraced spreading, at sufficiently strong solid-fluid interaction strengths, but did not give the "diffusive" growth rate seen experimentally. It appears then that the molecule size is an important parameter in the spreading rate. Other groups [9,11,12] have found diffusive spreading rates with or without chain molecules, but we have insisted on simulating a substrate with a realistic atomic structure and used a physically reasonable thermostatting procedure that mimics a laboratory experiment.

As the spreading proceeds, the strong substrate attraction draws the monomers toward the preferred sites at the minima of the substrate potential, while competition with the other chains produces an excluded volume effect that tends to elongate the chains, in terms of their radius of gyration and nearest-neighbor bond angles. The chains show an incomplete degree of commensurate alignment with the solid lattice due to a deliberate (and realistic) choice of incommensurate solid-solid and fluid-fluid potentials. Furthermore, the molecules are transiently localized at the preferred sites but not bound there, since while the thermal diffusivity is reduced compared to the free-fluid value, it is nonzero at least for the rather comparable liquid-liquid and liquid-solid interactions used here.

The layer dynamics provides some qualitative support to the impermeable pancake picture of de Gennes and Cazabat. The mass transfer between layers is quite reasonably largest at the layer edges, where the density is smallest, the molecules mobility is greatest, and the number of vacant sites largest. For the sizes amenable to simulation using these techniques, there is some mass transfer throughout the layers and there is motion in all

three directions. Unfortunately, it is not possible to extrapolate convincingly to much larger sizes and test the model's prediction that the interlayer motion is confined to an outer annular ring.

More generally, this work shows how molecular simulation, in concert with other techniques, can help unravel phenomena in which nontrivial microscopic aspects emerge. We expect that further simulations can consider such issues as the effects of surface roughness, the nature of the transitions between terraced and "ordinary" complete wetting, entanglement effect for longer polymer chains, more detailed interaction potentials, and so on.

ACKNOWLEDGMENTS

The research of J.D.C. and U.D.O. is supported by the Belgian Program on Interuniversity Poles of Attraction, initiated by the Belgian State, Prime Minister's Office, Science Policy Programming, by the Région Wallonne, and by Fond National de la Recherche Scientifique. J.K. and J.R.B. are supported by the U.S. National Science Foundation and National Aeronautics and Space Administration, with computer time provided by the Pittsburgh Supercomputer Center and the Goddard Space Flight Center.

[1] F. Heslot, A. M. Cazabat, P. Levinson, and N. Fraysse, Phys. Rev. Lett. **65**, 599 (1990).
[2] F. Heslot, N. Fraysse, and A. M. Cazabat, Nature **338**, 640 (1989).
[3] F. Heslot, A. M. Cazabat, and P. Levinson, Phys. Rev. Lett. **62**, 1286 (1989).
[4] J. De Coninck, S. Hoorelbeke, M. P. Valignat, and A. M. Cazabat, Phys. Rev. E **48**, 4549 (1993).
[5] J. De Coninck, Colloids Surf. A **80**, 131 (1993).
[6] J. De Coninck, N. Fraysse, M. P. Valignat, and A. M. Cazabat, Langmuir **9**, 1906 (1993).
[7] J. X. Yang, J. Koplik, and J. Banavar, Phys. Rev. Lett. **67**, 3539 (1991).
[8] J. X. Yang, J. Koplik, and J. Banavar, Phys. Rev. A **46**, 7738 (1992).
[9] J. Nieminen, D. Abraham, M. Karttienen, and K. Kaski, Phys. Rev. Lett. **69**, 124 (1992).
[10] J. De Coninck, U. D'Ortona, J. Koplik, and J. Banavar, Phys. Rev. Lett. **74**, 928 (1995).
[11] J. A. Nieminen and T. Ala-Nissila, Phys. Rev. E **49**, 4228 (1994).
[12] L. Wagner (unpublished).
[13] P. G. de Gennes and A. M. Cazabat, C. R. Acad. Sci. **310**, 1601 (1990).
[14] D. B. Abraham, J. De Coninck, F. Dunlop, and P. Collet, Phys. Rev. Lett. **65**, 195 (1990).
[15] J. M. Haile, *Molecular Dynamics Simulation: Elementary Methods* (Wiley, New York, 1993).